JOURNAL OF ATMOSPHERIC AND OCEANIC TECHNOLOGY

A report on progress on Corrected Moments in Antenna Coordinates 2.0

SCOTT COLLIS* AND JONATHAN HELMUS

Environmental Science Division, Argonne National Laboratory

ABSTRACT

In 2010 the Atmospheric Radiation Measurement program procured a number of 3 and 5cm wavelength radars for documenting the macrophysical, microphysical and dynamical structure of precipitating systems. In order to maximize the scientific impact the program supported the development of an application chain to correct for various phenomena in order to retrieve the "point" values of moments of the radar spectrum and polarimetric measurements. This report details the motivation, science and progress to date as well as charting a path forward.

1. Introduction

The Atmospheric Radiation Measurement Program (Mather and Voyles (2012)) (ARM) has a long history of sensing clouds in the column using the Millimeter Cloud Radar (MMCR, Now Ka-Band Zenith Radar or KaZR). Starting in 2010 ARM embarked on program to better characterize the domain surrounding the column using scanning radars at millimeter and centimeter wavelengths. Processing for the shorter wavelengths has been previously published Kollias et al. (2013) this report is limited to 5 and 3cm wavelengths. Due to the agility and lower cost per radar the program opted not to operate the common wavelength of 10cm (S-Band) which is robust to liquid water path attenuation in all but the most severe storms. This necessitates the development of robust code for the correction of issues due to the two way propagation of the radar through medium that both scatters and attenuates. In addition, the trade off between wavelength, maximum unambiguous range and Doppler nyquist velocity means the radars alias at 12.4 and 16.52 ms^{-1} for 3 and 5cm respectively when operating in a baseline mode (such as during the Mid-Latitude Convective Continental Clouds Experiment MC^3E (Jensen et al. (2015)). Due to extreme velocities of scatterers aloft and, in places such as Oklahoma, at the surface, aliasing is common and requires post moment calculation dealiasing. There are many techniques for dealiasing Doppler velocities (eg James and Houze (2001)) however on testing we found these techniques to be either difficult to implement in an operational chain or lacking in robustness.

When we first attempted to build a processing chain each step made its own decision on where to conditionally run based on various measurements of "quality" such as the co-polar (zero lag) correlation coefficient ρ_{HV} and Normalized Coherent Power (NCP, also referred to as Signal Quality Index or SQI). These are defined as:

$$\rho_{HV}(0) = \frac{|<S_{VV}S_{hh}^{*}>|}{\sqrt{<|S_{HH}|^2><|S_{VV}|^2>}} \quad (1)$$

$$NCP = \frac{P_{coh}}{P_{DC}}. \quad (2)$$

Where the S terms are elements of the scattering matrix, P_{coh} is the coherent part of the doppler spectrum and P_{DC} is the incoherent part. Since ARM radars use magnetron transmitters the phase is randomized from pulse to pulse so when a first trip return is mixed with a return from a scatterer beyond the maximum unambiguous range the derived radar Doppler spectrum when averaged over many pulses is flat and the NCP is low. While the Doppler spectrum from a first trip has structure from which (depending on the method) a peak can be found and Doppler velocity determined and the NCP approaches 1.0. However, the usefulness of NCP alone in second trip detection breaks down in regions of high spectral width. When the spectral width approaches the nyquist velocity, even in areas of purely first trip, the NCP decreases. This is especially troublesome in regions of high convergence and divergence in convective storms, often causing false flagging of these regions.

To overcome the issues of arbitrary decision making and faults in using NCP alone to detect multiple trips our application chain, Corrected Moments in Antenna Coordinates first attempts to identify the nature of the scattering medium at the gate. This gate-ID is performed before any

**Corresponding author address:* Scott Collis, Argonne National Laboratory, Environmental Science division, 9700 South Cass Ave, Argonne, IL 60514
E-mail: scollis@anl.gov

corrections are applied so it is different to hydrometeor identification codes (eg Dolan and Rutledge (2009), Wen et al. (2015), Al-Sakka et al. (2013) etc.) that seek to gain microphysical insight. Gate-ID is performed for the purpose of objectively determining where future algorithms should be applied. Since we are implementing CMAC2.0 using the Python-ARM Radar Toolkit (Py-ART, Heistermann et al. (2014)) we can use the the identifications to construct a gate filter.

2. Application chain

There exists many algorithms in the scientific literature for the quality control and correction of radar data. Far to many to adequately asses and implement. However, given Py-ART's data model driven approach it is possible to design an application chain that is highly modular and task based. Each component has a particular job and can be replaced as better algorithms are published (and, ideally, code shared). As stated in the previous section, the overarching idea behind CMAC2.0 is a gate-ID is created and determines the conditional application of algorithms. At the time of writing implemented classes are: Rain, melting layer, ice, second trip and no significant scatterer. Dealiasing, for example would run on the set of all classes except "no significant return" while retrievals of specific attenuation would run on the class of "rain". This approach requires that the gate-ID is run on the pre-corrected data. However, as discussed in sec 1, radar provided measurements alone are not sufficient to constrain the problem of gate-ID, especially the identification of multiple trips. There are a number of pre-ID retrievals and inputs we can generate to constrain the problem, however, and these are described in a.

The Application chain for CMAC2.0 is shown in fig 1 and can be broken down to:

- Pre-ID calculations of texture and mapping sounding data to radar gates
- Ascribing membership functions to gate classes, scoring of gates and classification at the gate of predominate scatterer.
- Dealiasing of Doppler velocities.
- Extraction of propagation differential polarimetric phase from instrument measured differential polarimetric phase.
- Calculation of specific differential phase.
- Calculation of specific attenuation.
- Integrate and apply to reflectivity.
- Calculate rain rate for liquid precipitation using specific attenuation.

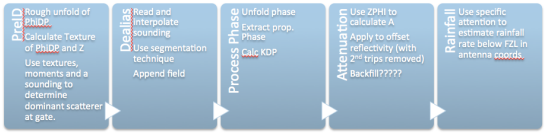

FIG. 1: The Application chain for Corrections in Antenna Coordinates 2.0

a. Calculations performed to aid identification of scatterers at gate

There are two steps to add information in order to determine dominant scattering process at the gate: Mapping temperature to gate locations and using texture of radial velocity as a discriminant of significant scattering.

Since Py-ART already ascribes a cartesian displacement from the radar for each gate using a simple $\frac{4}{3}R_e$ standard atmosphere propagation model CMAC2.0 simply interpolates sonde data available from ARM soundings (via the interpolated sonde product DOI).

The idea behind texture is that when second trips (or no-trips) dominate, due to the pulse-to-pulse randomized phase of a magnetron transmitter, radial velocity should vary, from gate to gate, between nyquist and negative nyquist randomly. As long as there is some structure to the radar Doppler spectrum the signal processor should be able to pick a peak and determine the 1st moment being the radial velocity. Thus the gate-to-gate and azimuth to azimuth variation, or texture of Doppler velocity should be able to act as a good discriminant of significant returns. The abstract concept is for a central pixel, (i,j) in 4, the points surrounding in a n by m kernel are collected then the statistic (eg variance) is calculated on the set of points and is returned as the (i,j)th value in the resultant 2D (range, time/azimuth) array.

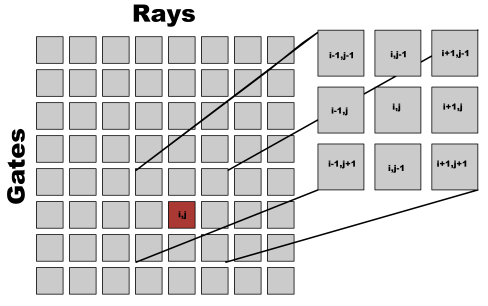

FIG. 2: Illustration of the concept of a moving filter over range gates of adjacent rays. The center element, (i,j) is calculated by passing surrounding elements. The footprint of the surrounding elements is determined by the kernel. In many cases we use a 3x3 kernel

The challenge comes from the desire to calculate this pre-correction. Doppler folding will generate a significant signal in the texture field if done purely on radial velocity values. However projection of radial velocity values onto a unit circle allows a smooth transition from positive nyquist to negative nyquist and there is a branch of mathematics dealing with the statistics of directions and magnitudes known as directional statistics (Wikipedia (2016)). Values from positive nyquist to negative nyquist are projected onto a circle with $\theta = 0$ to π and the standard deviation is given by:

$$x = \cos\theta \tag{3}$$
$$y = \sin\theta \tag{4}$$
$$R = \sqrt{\bar{x}^2 + \bar{y}^2} \tag{5}$$
$$S = \sqrt{-2 * \log R} \tag{6}$$

Figure 3a shows a typical radial velocity field, with folds, from the ARM C-SAPR at the Southern Great Plains. Figure 3b shows the texture field calculated by passing eq. 6 over data in 3a using a 3x3 kernel as shown in fig 4.

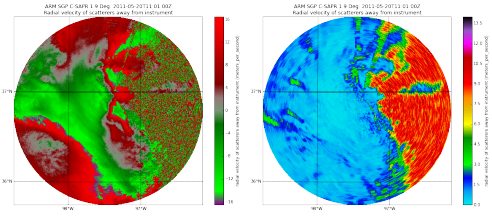

(a) Radial velocity (b) Texture

FIG. 3: Calculations of texture of radial velocity from the C-Band Scanning ARM Precipitation Radar (C-SAPR) using circular statistic to avoid false texture on folds

There are clearly higher values of texture where there are no significant returns while texture falls quickly over the precipitation echo boundaries. However the exact values of texture to be used in the membership function to delineate between significant and non-significant will depend on many factors that influence texture including number of samples, signal to noise etcetera. Plotting a histogram of texture values yields two distinctly separated populations of gates. To find the discrimination point we use Scientific Python's (Jones et al. (2001–)) continuous wavelet transform-based peak finding algorithm (Du et al. (2006)) to find the location of the left and right peak. The cut off is then decided by finding the minimum value, or valley, between the two peaks. Ad-hoc testing shows this to be robust even when changing radar types. We tested with X,C and Ka band radars all using different configurations.

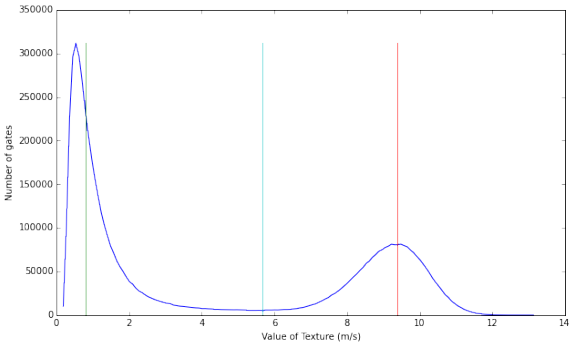

FIG. 4: Histogram of texture values from the volume shown in fig 3a. The left hand peak corresponds to significant returns, the right hand to noise. The black and red lines are the peak center guess by a wavelet based technique. The green line is the minimum value between the two peaks.

b. Fuzzy logic based identification of scatterers at gate

As previously discussed the aim of this step is to identify the dominant scatterer at each gate to aid in decision making upchain. While fuzzy logic has been used for particle identification extensively few investigators have done this as a first step (pre K_{dp} etc). A Notable exception is work by Gourley et al. (2007). Preprocessing ID depends on using the moments and derived products assuming they contain all the issues associated with unprocessed data. We use a simple scheme which associates a membership with each classification of: Melting layer, Multi-trip, Rain and Snow. We have future plans to include gates that are contaiminated by hail in the propagation path. Membership functions are shown in table 1. At the moment, with the exception of texture as referenced in sec a, these are determined using trail and error. As we have set up a robust codebase using Py-ART and Scikits Fuzzy we can revisit the membership functions at any time using better formulations determined using mixtures of machine learning and other techniques.

Figure 5 shows an example of scatterer at gate identification from the 1.9 degree PPI tilt from the C-SAPR during MC3E as a organized linear convective system passed over the site. Regions of snow scatterers are shown in cyan, rain in green, multi-trip in red, mixed scattering in yellow (eg melting layer) and no significant return in grey. Work is proceeding on determining if a radial is hail contaminated as is work on clutter identification and tagging. Figure 6 shows an example of scatterer at gate identification from the 37.3 degree horizon to horizon RHI from the X-SAPR during for the stratiform region of the same system. The high elevation "stripe" is an artifact likely caused by near field distortion of the antenna pattern by a metal

TABLE 1: Inputs for trapezoidal membership functions for various classes

Class	Tex (m/s)	ρ_{HV}	NCP	Temperature (C)	height (km)	SNR (dB)
melting	[0, 0, 4, 6], 1.5	[0.6, 0.65, 0.9, 0.96], 3.5	[0.4, 0.5, 1, 1], 0	[0, 0.5, 6, 7], 1	[0, 0, 25, 25], 0	[8, 10, 1000, 1000], 0
multi trip	[5, 6, 130, 130], 5	[0.5, 0.7, 1, 1], 0	[0, 0, 0.5, 0.6], 0	[-100, -100, 100, 100], 0	[0, 0, 5, 8], 0	[15, 20, 1000, 1000], 1
rain	[0, 0, 4, 6], 1	[0.97, 0.98, 1, 1],1	[0.4, 0.5, 1, 1], 1	[2, 5, 100, 100], 2	[0, 0, 5, 6], 0]	[8, 10, 1000, 1000], 1
snow	[0, 0, 4, 6], 1	[0.65, 0.9, 1, 1],1	[0.4, 0.5, 1, 1], 1	[-100, -100, 0.5, 4], 2	[0, 0, 25, 25], 0	[8, 10, 1000, 1000], 1

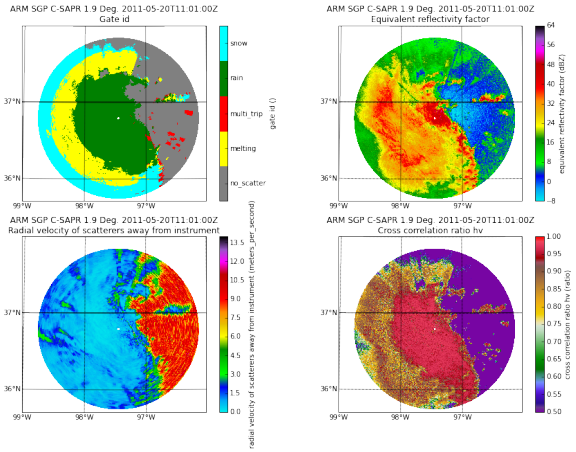

FIG. 5: Highest score determined categories with hard constraints for the dominant scattering process for each gate from the C-SAPR alongside with (clockwise) reflectivity factor, Texture and cross correlation ratio. These values will be used to determine what post-processing will be applied gate-to-gate.

object (powerline) causing the bright band to be present at those angles.

Gate, or scatter ID, is used to form Py-ART Gate-filter objects which can be the passed to subsequent processing algorithm. For example Linear programming (see sec 2) filtering of ϕ_{DP} would be performed gates identified as rain and attenuation correction (offset) on the union of rain, melting layer and snow.

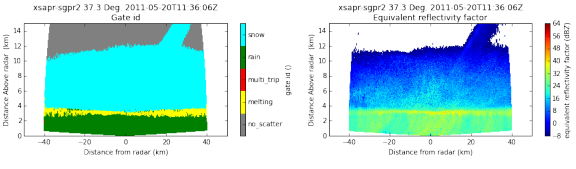

FIG. 6: Highest score determined categories with hard constraints for the dominant scattering process for each gate from the X-SAPR alongside with reflectivity factor

c. *Corrections and retrievals*

In order to have the greatest impact to stakeholders the ARM radars need to provide high quality calibrated and corrected moments and measurements. By measurements we mean the *intrisnsic* value. That is the measurement corrected for all the issues of propagation and processing. In CMAC2.0 this means:

- Dealiased doppler velocities
- ϕ_{DP} corrected for non-uniform beam filling and phase shift on backscatter
- Specific differential phase K_{DP}
- Specific Attenuation
- Reflectivity corrected for liquid water path attenuation

1) DEALIASING

Originally the Four Dimensional Dealiasing, (4DD, James and Houze (2001)) was wrapped into Py-ART using NASA's Radar Software Library (RSL). Issues with the implementation of the paper into code led to a long discussion on issues in Dealising (see https://github.com/ARM-DOE/pyart/issues/119). Discussions led to two new solutions in doppler velocity unfolding: Fringe pattern based and region based. Unlike the dealiasing of cloud radar data where it can be assumed scatterers move purely with the wind storm dynamics creates radial velocity patterns that can move counter flow. The fringe or "phase based" technique is an image analysis technique designed for removing fringe patters from interferometric images. Early tests were sub-par and while the technique is added to Py-ART it is rarely used. The region based technique performs Doppler velocity dealiasing by finding regions of similar velocities and unfolding and merging pairs of regions until all regions are unfolded. Unfolding and merging regions is accomplished by modeling the problem as a dynamic network reduction. Figure 7 shows raw and unfolded radial velocities from the ARM C-SAPR radar collected during MC3E. Unfolding

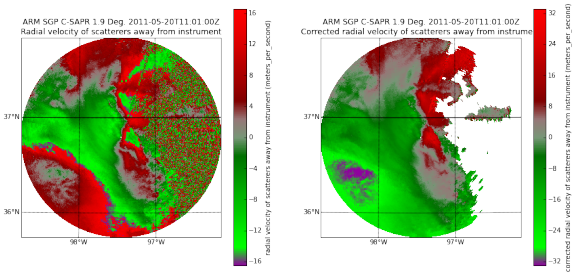

FIG. 7: Raw and dealiased radial velocities from the ARM C-SAPR radar collected during MC3E. Unfolding was performed using the region based approach.

was performed using the region based technique. Since the technique has been optimized it takes just under 10 seconds to compete a full volume like the one shown given an appropriate gatefilter is provided. Currently the algorithm does not require a sounding, so it will unfold to the nearest whole nyquist interval. In the rare occasion where the whole scene is moving in bulk at above a nyquist the unfolding will be incorrect but simply fixed by minimizing compared to a synthetic volume generated by a sounding. Long term testing of the algorithm is underway in collaboration with the University of Barcelona and the Catalan Meteorological Service.

2) FILTERING OF MEASURED PHASE SHIFT BETWEEN VERTICAL AND HORIZONTAL POLARIZATION

Raw polarimetric phase shift Ψ_{DP} can be broken down into a component due to differential liquid water path (Φ_{DP}) and other, specific terms, due to partial beam filling (NBF) and phase shift on backscatter (δ). Mathematically:

$$\Psi_{DP} = \Phi_{DP} + \delta + NBF \tag{7}$$

see Giangrande and Ryzhkov (2008) and references therein. In order to extract microphysical insight into the liquid (precipitating) liquid water path it is desirable to retrieve Φ_{DP} from the measured signal. Taking advantage of the fact that liquid water content can not be negative and therefore we expect Φ_{DP} do be strictly increasing we can construct a filter to extract Φ_{DP} from Ψ_{DP}. Giangrande et al. (2013) outlines an objective technique that uses Linear Programming (LP, see, for example, HELBUSH (1968)) to create a Φ_{DP} that is piecewise increasing and (importantly) is non-biased. That is, given a Ψ_{DP} that contains a smoothly increasing signal and a short term variation the algorithm will fit through the base rather than the mid-point or peak of the variation. The strength of the fit is influenced by the local reflectivity as a weak constraint. Where reflectivity is high positivity in the gradient of Φ_{DP} is enforced (see Giangrande and Ryzhkov (2008) for details). Once Φ_{DP} is retrieved the specific differential phase, K_{DP} is retrieved by convoluting Φ_{DP} with a 20 point linear ramp (a sobel filter). This is similar in nature and adhoc experimentation shows it to closely mimic a moving linear fit similar to that used in Bringi et al. (2002).

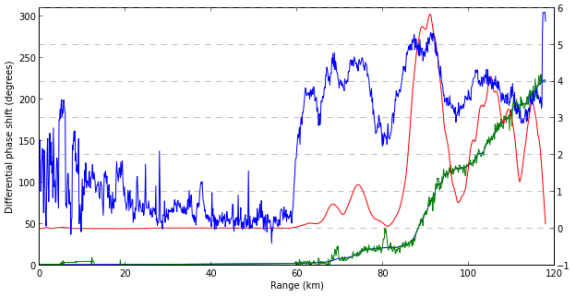

FIG. 8: A single radial of data from C-SAPR highlighting the LP technique. Raw Ψ_{DP} is shown in green, retrieved Φ_{DP} in black, K_{DP} in red and reflectivity (divided by 10) in blue.

Figure 8 shows a single radial of data from C-SAPR highlighting the LP technique. Raw Ψ_{DP} is shown in green, retrieved Φ_{DP} in black, K_{DP} in red and reflectivity (divided by 10) in blue. The retrieved Φ_{DP} is strictly increasing resulting in a strictly positive K_{DP}. LP minimization is achieved by using the CoinLP library. Initially PyGLPK was used but with a very welcome contribution to Py-ART from Kai Mühlbauer from the University of Bonn switching to CoinLP reduced volume processing time from 8 minutes to under a minute.

3) RETRIEVAL OF SPECIFIC ATTENUATION

Specific attenuation, A was retrieved using an adaptation of an iterative "hotspot" method as outlined in Gu et al. (2011). Using the aforementioned gate ID a gatefilter is constructed that only calculates A in regions of liquid precipitation assuming attenuation due to ice is negligible and in mixed phase regions intractable. Occasionally clutter can throw off the adaptive technique creating hotspots where none occur. While not much of an issue for specific attenuation

3. Challeges

The data u

4. Future work

The climatology and varianc

Acknowledgments. Scott G
Patricia

References

Al-Sakka, H., A.-A. Boumahmoud, B. Fradon, S. J. Frasier, and P. Tabary, 2013: A New Fuzzy Logic Hydrometeor Classification Scheme Applied to the French X-, C-, and S-Band Polarimetric Radars. *Journal of Applied Meteorology and Climatology*, **52 (10)**, 2328–2344, doi:10.1175/JAMC-D-12-0236.1, URL http://journals.ametsoc.org/doi/abs/10.1175/JAMC-D-12-0236.1.

Bringi, V. N., G.-J. Huang, V. Chandrasekar, and E. Gorgucci, 2002: A Methodology for Estimating the Parameters of a Gamma Raindrop Size Distribution Model from Polarimetric Radar Data: Application to a Squall-Line Event from the TRMM/Brazil Campaign. *Journal of Atmospheric and Oceanic Technology*, **19 (5)**, 633–645, doi:10.1175/1520-0426(2002)019⟨0633:AMFETP⟩2.0.CO;2, URL http://journals.ametsoc.org/doi/abs/10.1175/1520-0426%282002%29019%3C0633%3AAMFETP%3E2.0.CO%3B2.

Dolan, B., and S. A. Rutledge, 2009: A Theory-Based Hydrometeor Identification Algorithm for X-Band Polarimetric Radars. *Journal of Atmospheric and Oceanic Technology*, **26 (10)**, 2071–2088, doi:10.1175/2009JTECHA1208.1, URL http://journals.ametsoc.org/doi/abs/10.1175/2009JTECHA1208.1.

Du, P., W. A. Kibbe, and S. M. Lin, 2006: Improved peak detection in mass spectrum by incorporating continuous wavelet transform-based pattern matching. *Bioinformatics*, **22 (17)**, 2059–2065, doi:10.1093/bioinformatics/btl355, URL http://bioinformatics.oxfordjournals.org/content/22/17/2059.abstract, http://bioinformatics.oxfordjournals.org/content/22/17/2059.full.pdf+html.

Giangrande, S. E., R. McGraw, and L. Lei, 2013: An Application of Linear Programming to Polarimetric Radar Differential Phase Processing. *Journal of Atmospheric and Oceanic Technology*, **30 (8)**, 1716–1729, doi:10.1175/JTECH-D-12-00147.1, URL http://journals.ametsoc.org/doi/abs/10.1175/JTECH-D-12-00147.1.

Giangrande, S. E., and A. V. Ryzhkov, 2008: Estimation of rainfall based on the results of polarimetric echo classification. *Journal of Applied Meteorology and Climatology*, **47 (9)**, 2445–2462, doi:10.1175/2008JAMC1753.1, URL http://dx.doi.org/10.1175/2008JAMC1753.1, http://dx.doi.org/10.1175/2008JAMC1753.1.

Gourley, J. J., P. Tabary, and J. Parent du Chatelet, 2007: A Fuzzy Logic Algorithm for the Separation of Precipitating from Nonprecipitating Echoes Using Polarimetric Radar Observations. *Journal of Atmospheric and Oceanic Technology*, **24 (8)**, 1439–1451, doi:10.1175/JTECH2035.1, URL http://journals.ametsoc.org/doi/abs/10.1175/JTECH2035.1.

Gu, J.-Y., A. Ryzhkov, P. Zhang, P. Neilley, M. Knight, B. Wolf, and D.-I. Lee, 2011: Polarimetric Attenuation Correction in Heavy Rain at C Band. *J. Appl. Meteor. Climatol.*, **50 (1)**, 39–58, doi:10.1175/2010JAMC2258.1, URL http://journals.ametsoc.org/doi/abs/10.1175/2010JAMC2258.1.

Heistermann, M., and Coauthors, 2014: The Emergence of Open Source Software for the Weather Radar Community. *Bull. Amer. Meteor. Soc.*, doi:10.1175/BAMS-D-13-00240.1, URL http://journals.ametsoc.org/doi/abs/10.1175/BAMS-D-13-00240.1.

HELBUSH, R. E., 1968: Linear programming applied to operational decision making in weather risk situations. *Monthly Weather Review*, **96 (12)**, 876–882, doi:10.1175/1520-0493(1968)096⟨0876:LPATOD⟩2.0.CO;2, URL http://dx.doi.org/10.1175/1520-0493(1968)096⟨0876:LPATOD⟩2.0.CO;2, http://dx.doi.org/10.1175/1520-0493(1968)096⟨0876:LPATOD⟩2.0.CO;2.

James, C. N., and R. A. Houze, 2001: A Real-Time Four-Dimensional Doppler Dealiasing Scheme. *Journal of Atmospheric and Oceanic Technology*, **18 (10)**, 1674–1683, doi:10.1175/1520-0426(2001)018⟨1674:ARTFDD⟩2.0.CO;2, URL http://journals.ametsoc.org/doi/abs/10.1175/1520-0426(2001)018%3C1674%3AARTFDD%3E2.0.CO%3B2.

Jensen, M. P., and Coauthors, 2015: The Midlatitude Continental Convective Clouds Experiment (MC3e). *Bulletin of the American Meteorological Society*, doi:10.1175/BAMS-D-14-00228.1, URL http://dx.doi.org/10.1175/BAMS-D-14-00228.1.

Jones, E., T. Oliphant, P. Peterson, and Coauthors, 2001–: SciPy: Open source scientific tools for Python. URL http://www.scipy.org/, [Online; accessed 2016-03-02].

Kollias, P., and Coauthors, 2013: Scanning ARM Cloud Radars. Part II: Data Quality Control and Processing. *Journal of Atmospheric and Oceanic Technology*, **31 (3)**, 583–598, doi:10.1175/JTECH-D-13-00045.1, URL http://dx.doi.org/10.1175/JTECH-D-13-00045.1.

Mather, J. H., and J. W. Voyles, 2012: The Arm Climate Research Facility: A Review of Structure and Capabilities. *Bull. Amer. Meteor. Soc.*, **94 (3)**, 377–392, doi:10.1175/BAMS-D-11-00218.1, URL http://journals.ametsoc.org/doi/abs/10.1175/BAMS-D-11-00218.1.

Wen, G., A. Protat, P. T. May, X. Wang, and W. Moran, 2015: A Cluster-Based Method for Hydrometeor Classification Using Polarimetric Variables. Part I: Interpretation and Analysis. *Journal of Atmospheric and Oceanic Technology*, **32 (7)**, 1320–1340, doi:10.1175/JTECH-D-13-00178.1, URL http://dx.doi.org/10.1175/JTECH-D-13-00178.1.

Wikipedia, 2016: Directional statistics — wikipedia, the free encyclopedia. URL https://en.wikipedia.org/w/index.php?title=Directional_statistics&oldid=705952853, [Online; accessed 1-March-2016].